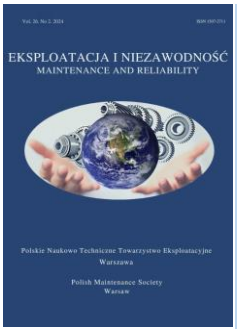

Eksploatacja i Niezawodnosc – Maintenance and Reliability

Volume 26 (2024), Issue 2

journal homepage: http://www.ein.org.pl

Article citation info:
Zhang Z, Lv X, Qi B, Qi Y, Zhang M, Tao Z, Surface roughness prediction and roughness reliability evaluation of CNC milling based on surface topography simulation, Eksploatacja i Niezawodnosc – Maintenance and Reliability 2024: 26(2) http://doi.org/10.17531/ein/183558

Surface roughness prediction and roughness reliability evaluation of CNC milling based on surface topography simulation

Indexed by: Web of Science Group

Ziling Zhang[a,*], Xiaodong Lv[a], Baobao Qi[b,c], Yin Qi[d], Milu Zhang[a], Zhiqiang Tao[e]

[a] Logistics Engineering College, Shanghai Maritime University, Shanghai, 201306, China
[b] Key Laboratory of CNC Equipment Reliability, Ministry of Education, Jilin University,130000, China
[c] Key Laboratory of Advanced Manufacturing and Intelligent Technology for High-end CNC Equipment,130000, China
[d] Yingtan Advanced Technical School, Jiangxi 335000, China
[e] College of Robotics, Beijing Union University, Beijing, 100027, China

Highlights

- A milling surface topography model was developed based on milling kinematics theory.
- A surface roughness prediction model is proposed based on the sparrow search algorithm optimized least support square vector machine method.
- A surface roughness reliability model is presented based on response surface methodology.
- The correctness of the proposed method is verified by milling experiments on 7050 aluminium alloy.

Abstract

Surface roughness is influenced by various factors with uncertainty characteristic, and roughness reliability can be used for the assessment of the surface quality of CNC milling. The paper develops a method for the assessment of surface quality by considering the coupling effect and uncertainty characteristics of various factors. According to the milling kinematics theory, the milling surface topography simulation is conducted by discretizing the cutting edge, machining time, and workpiece. Considering the coupling effect of various factors, a roughness prediction model is established by the SSA-LSSVM, and its prediction accuracy reaches more than 95%. Then, the roughness reliability model is developed by applying the response surface methodology to achieve the assessment of surface quality. The proposed method is verified by the milling experiments. The maximum values of the relative errors between the simulation and experimental results of the surface roughness and roughness reliability are 9% and 1.5% respectively, indicating the correctness of the method proposed in the paper.

Keywords
surface roughness reliability, SSA-LSSVM, response surface methodology, surface quality, CNC milling

1. Introduction

With the rapid development of manufacturing technology, the surface integrity of parts has received great attention in related fields. The formation mechanism of surface geometries and the modeling process are important components of surface integrity studies, which mainly includes irregular micro-geometries such as surface roughness, waviness, and shape error [1]. The formation of surface topography of the part is a complex process, it is through the relative motion of the tool on the surface of the workpiece to remove the material to form different shapes and sizes of bumps and valleys. From this point of view, tool parameters and machining parameters have a great influence on the surface topography, which further affects the mechanical and usage properties of the workpiece as well as the working accuracy and life [2]. Milling is widely used in the field of CNC

(*) Corresponding author.
E-mail addresses: Z. Zhang (ORCID: 0000-0001-8132-5744) zhangziling1119@126.com, X. Lv lxd202130210033@163.com, B. Qi qibaobao@jlu.edu.cn, Y. Qi kylin8642@163.com, M. Zhang zhangmilu@126.com, Z. Tao (ORCID: 0000-0001-5654-4005) jqrzhiqiang@buu.edu.cn

machining, in which the ball end milling cutter is usually applied to CNC milling for machining typical parts due to its adaptability and easy planning of machining routes. Therefore, the research on the surface quality of CNC milling machining has arisen, in which how to perform surface topography simulation and roughness prediction of the workpiece is the core task.

Nowadays, many investigators have done deep studies about milling surface topography and obtained some worthwhile theories and methods. Depending on the dynamic response, Yuan et al [3] established a cylindrical milling cutter milling workpiece surface topography simulation model. Peng et al [4] studied the prediction and simulation of 3D surface morphology based on microsphere end milling. Zhang et al [5] proposed the surface morphology model with the initial phase difference as a variable in milling and analyzed its effect on the surface morphology characteristics. Zhang et al [6, 7] researched the surface topography acquired by rounded corner milling cutters under multi-axis control. Paper [8,9] established the model of surface topography with the Z-map method. Żurawski K et al [10] presented a method for predicting the surface topography by taking into account the depth and width of cutting as well as radial runout, which was validated by milling experiments of three different materials. Chen et al [11] presented a method for surface morphology formation during vibration-assisted milling. Corral et al [12] developed a mathematical model of surface topography based on the geometrical intersection of the tool and the workpiece. Paper [13,14] investigated the effects of feed rate and tool inclination changes on surface morphology and proved the feasibility of the method by three-axis milling experiments.

As one of the important indexes of surface geometry, it is especially essential to accurately establish the prediction model of surface roughness. For the past few years, various academics have done research on the prediction of surface roughness. Agrawal et al [15] conducted 39 sets of turning machining AISI 4340 steel tests on machine CNC machine tools and used multiple linear regression methods to establish a model of the surface roughness. Kong et al [16] comprehensively analyzed the advantages and disadvantages of four Bayesian linear regression models in predicting surface roughness and provided an accurate method to predict roughness. Shahrajabian et al [17] obtained the relationship between surface roughness and machining parameters using orthogonal tests, which were optimized by a genetic algorithm to obtain the parameters corresponding to the minimum surface roughness. Ouyang et al [18] investigated the surface roughness prediction problem during milling machining based on BP neural network algorithm. Han [19] developed a prediction model for the surface roughness of metal-formed parts, and it was concluded that the surface roughness increases with the increase of contact normal pressure by the model. Liu et al [20] established the surface roughness prediction model for ball screw whirlwind milling according to Hertz's elastic contact theory and argued that the surface roughness is inversely proportional to the cutting force under the same cutting parameters. Considering the high-speed precision milling, Li [21] built a roughness prediction model in the high-speed milling process by optimizing lssvm with particle swarm algorithm. Nevertheless, with the development of intelligent algorithms, the use of time series modelling for prediction is becoming more common. The paper provides an overview of the recent literature on time series modelling, as shown in Table 1.

Table 1. The literature and method for correlated time series modelling.

Modelling methods	Relevant literature	Field of application
LSTM-ALO; LSTM-INFO	[22-24]	Evaluation of battery health life; Prediction of water flow
RVM-IMRFO	[25]	Evaluation of variables; monthly pan evaporation prediction
ANFIS-WCAMFO	[26]	Water resources management, agricultural planning and irrigation design
ELM-JFO	[27]	Modelling groundwater level fluctuations
SVM–FFAPSO	[28]	Urban water planning and management

The papers [22-24] used a correlation time series algorithm to evaluate the battery life and to predict water flow rate, respectively. Paper [25] proposed an RVM-IMRFO model to predict monthly pan evaporation with limited climatic data (e.g., temperature). To address the problem of difficult selection of hyperparameters in adaptive neuro-fuzzy inference systems (ANFIS), paper [26] applied the WCA-MFO to seek optimization of parameters in ANFIS and applied this hybrid algorithm to achieve the prediction of reference evapotranspiration, which is of vital importance for water resources management and agricultural planning. Adnan R M et al [27] used the ELM-JFO algorithm to develop a prediction model for groundwater levels by using hydroclimatic numbers. The articlethe fully utilizes

JFO algorithm's strong optimization ability and fast convergence speed to solve the problem of ELM's difficulty in finding a global optimized solution. Paper [28] used the FFA algorithm to compensate for the PSO algorithm's weakness of easily falling into local optimum, and combined them with the SVM method to evaluate the dissolved oxygen concentration, which is of great significance for drinking water resources as well as aquatic ecology. These correlated time series algorithms mainly predict the future trends based on existing historical data. For example, the prediction of water flow and the prediction of evapotranspiration in the above study. These forecasting problems are to some extent related to time as well as seasonal variations and can be further divided into long-term time and short-term time prediction. The above articles are of the great value and have an important contribution to the modelling of the relevant aspects of time series. However, in the paper, the data used to build the surface roughness prediction model is obtained from a surface topography simulation model. With a specific set of parameters, a specific surface roughness value can be attained. The data of the previous moment does not influence the data of the subsequent moment and the modelling process has no relation to the order of data selection. Therefore, the paper does not use correlation time series modelling approach to develop the surface roughness prediction study. In addition, regression prediction method is usually employed to solve the problem of surface roughness prediction, such as multiple regression [15,17,30], random forest regression [15,31], bayesian linear regression [16], least squares support vector machine regression [21,29]. However, some parameters involved in these regression methods are difficult to select and the problem of how to reasonably determine the form of the regression equation, which leads to the prediction model accuracy does not meet the requirements. Therefore, the paper utilizes the advantage of LSSVM in dealing with nonlinear regression problems and combines the powerful optimization searching ability of the sparrow search algorithm to establish a surface roughness prediction model of SSA-LSSVM, aiming at solving the problem of the lack of surface roughness prediction accuracy.

The above studies are basically about milling surface topography and surface roughness prediction studies. On the one hand, most of the surface roughness prediction studies are conducted by designing orthogonal experiments, and the roughness prediction model is built with multiple regression, neural networks and other methods according to orthogonal experimental data. The models above do not completely consider the coupling effect of various parameters and the amount of data used for modeling is low, which greatly have an impact on the prediction accuracy of the model. On the other hand, in the practical machining, the uncertainty of surface roughness is caused by the uncertainty characteristics of the parameters, which has a great impact on the assessment of surface quality. These are not involved in the above studies on surface quality. Therefor, the paper aims to solve the above practical problems of low accuracy of surface roughness prediction and rational assessment of surface quality.

The paper established a milling surface topography simulation model based on milling kinematics, which comprehensively considers the coupling effect of each parameter. The model reveals the intrinsic mechanism of the milling process, and provides the basis for the establishment of the surface roughness prediction model; To realize the higher prediction accuracy of surface roughness, a full-factor simulation experiment with 4 parameters was used, and a total of 256 sets of data were obtained. SSA was used to optimize the parameters in the LSSVM, which overcame the problem of the difficulty in selecting the parameters in the LSSVM, so that the prediction accuracy and performance of the model were further improved; The paper established a roughness reliability model based on the response surface method, which provides a reference for solving the problem of surface quality uncertainty due to the uncertainty characteristics of parameters in the actual machining process. Hence, in the paper, a surface roughness prediction model and a universal method for the assessment of surface roughness are presented, which have the advantages as follows:

(1) Based on milling kinematics theory, a milling surface topography model is established by discretizing the milling edge and machining time. This model reveals the intrinsic mechanism of the milling process, and provides the basis for the establishment of the surface roughness prediction model.

(2) Considering the coupling effect of various factors, the surface roughness prediction model is developed based the SSA-LSSVM, which realises the prediction of surface roughness accurately and provides a foundation for roughness

reliability modelling.

(3) Due to the uncertainty characteristic of the parameters affecting surface roughness in actual machining, a surface roughness reliability model is built by the response surface methodology. The method expands the assessment of surface quality from the traditional deterministic analysis to the uncertainty analysis, which is closer to the actual mill machining process.

2. Milling surface topography modelling based on ball end milling cutter

2.1. Cutting edge model

To establish the milling surface topography model of the ball-end milling cutter, it is necessary to obtain the milling edge model first.

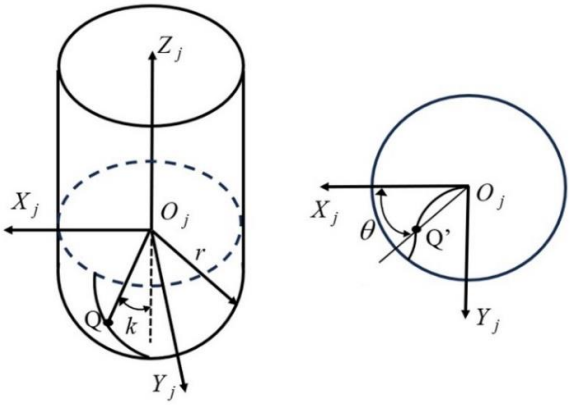

Fig.1. Cutting edge model of ball end milling cutter.

As shown in Fig. 1, the ball milling cutter *j*-th tooth local coordinate system *Oi-XiYiZi* is established, in which the ball centre is the origin and the axis *Zj* is coincident with the tool axis direction. Therefore, any point *Q* on the *j*-th tooth can be represented:

$$\begin{cases} Q_x = r\sin k \cdot \cos\theta \\ Q_y = r\sin k \cdot \sin\theta \\ Q_z = -r\cos k \end{cases} \quad (1)$$

Where r is the tool radius (unit: mm), k is the angle between the line connecting the *Q* point and the centre of the ball end milling cutter with the negative direction of the coordinate axis *OiZi* (unit: rad), θ is the angle from the line *Q'O* to the axis O_iX_i, where *Q'* is the projection point of the point *Q* on the plane O_i-X_iY_i, θ is related to the helix angle φ as shown below:

$$\theta = \tan\varphi \, ln(\cot(\tfrac{k}{2})) \quad (2)$$

Where φ is the helix angle.

Therefore, combining equations (1) and (2), the coordinates of any point *Q* on the *i*-th tooth in the cutter edge in the coordinate system *Oi-XiYiZi* can be expressed:

$$\begin{cases} Q_x = r\sin k \cdot \cos(\tan\varphi \, ln(\cot(\tfrac{k}{2}))) \\ Q_y = r\sin k \cdot \sin(\tan\varphi \, ln(\cot(\tfrac{k}{2}))) \\ Q_z = -r\cos k \end{cases} \quad (3)$$

2.2. Trajectory equation of cutting edge

To facilitate the establishment of the equations of the milling edge trajectory, the coordinate system based on the milling process of the ball-end cutter is established in Fig. 2. The description for each coordinate system is as follows:

a) O_G-$X_GY_GZ_G$ is the workpiece coordinate system, usually with the lower left corner of the workpiece as the coordinate origin, which is used to represent the interrelationship between the tool and the workpiece.

b) O_J-$X_JY_JZ_J$ is the tool spindle coordinate system, the coordinate axis O_JZ_J coincides with the machine tool spindle axis and performs a translational movement relative to the workpiece, which is in the same direction as the coordinate system O_G-$X_GY_GZ_G$.

c) O_C-$X_CY_CZ_C$ is the tool coordinate system, which is established with the ball centre of the tool as the origin. When the tool is not eccentric, the axis O_CZ_C is coincident with the axis O_JZ_J and rotates around the machine spindle with angular velocity ω.

d) The coordinate system O_D-$X_DY_DZ_D$, the same as Oi-XiYiZi above, is used to represent any point on the *j*-th tooth, whose coordinate axis O_DZ_D coincides with the coordinate axis O_CZ_C.

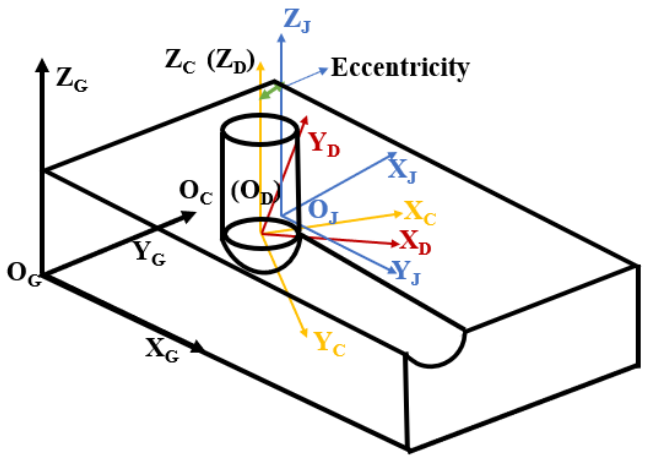

Fig. 2. Coordinate system in milling.

Double-edged and four-edged ball end milling cutters are commonly used in the milling process. One of the cutter teeth is designated as the reference cutter tooth and its coordinate system is consistent with the tool coordinate system. Thus, the coordinate transformation matrix from the coordinate system O_D-$X_DY_DZ_D$ to the coordinate system O_C-$X_CY_CZ_C$ can expressed:

$$T_{D-C} = \begin{bmatrix} \cos\beta & -\sin\beta & 0 & 0 \\ \sin\beta & \cos\beta & 0 & 0 \\ 0 & 0 & 1 & 0 \\ 0 & 0 & 0 & 1 \end{bmatrix} \quad (4)$$

where $\beta = (j-1)\cdot 2\pi/N$,and N is the total number of cutter teeth.

Due to the existence of tool eccentricity during milling, it is assumed that the eccentricity distance between the tool axis O_DZ_D and the spindle axis is e, and the radial eccentricity angle is δ; Assuming that the spindle drives the tool around the spindle coordinate system with an angular velocity ω to turn clockwise. Hence, taking into account the tool eccentricity, spindle rotation, and cutting tool attitude, the transformation matrix from O_C-$X_CY_CZ_C$ to O_J-$X_JY_JZ_J$ can be stated as:

$$T_{C-J} = \begin{bmatrix} \cos\eta & \sin\eta\cos\psi & -\sin\eta\sin\psi & e\cos\delta \\ -\sin\eta & \cos\eta\cos\psi & -\cos\eta\sin\psi & e\sin\delta \\ 0 & \sin\psi & \cos\psi & 0 \\ 0 & 0 & 0 & 1 \end{bmatrix} (5)$$

Where $\eta = \phi_0 - \omega t$, ϕ_0 is the initial phase angle, t is the processing time, and ψ is the forward tilt angle.

During the milling process, it is assumed that the displacements of the ball centre of the ball end milling cutter in the X, Y, and Z directions are x_d, y_d and z_d respectively, then the coordinate transformation matrix from O_J-$X_JY_JZ_J$ to O_G-$X_GY_GZ_G$ can be defined as:

$$T_{J-G} = \begin{bmatrix} 1 & 0 & 0 & x_0 + x_d \\ 0 & 1 & 0 & y_0 + y_d \\ 0 & 0 & 1 & z_0 + z_d \\ 0 & 0 & 0 & 1 \end{bmatrix} \quad (6)$$

Where x_d, y_d and z_d are the coordinates of the initial position of the ball centre for the ball end milling cutter in the workpiece's coordinate system.

Therefore, the transformation from the coordinate system O_D-$X_DY_DZ_D$ to the coordinate system O_G-$X_GY_GZ_G$ is all completed, and the equation of the trajectory of any point in the workpiece's coordinate system can be denoted as:

$$(X, Y, Z, 1) = T_{J-G}\cdot T_{C-J}\cdot T_{D-C}\cdot (Q_x, Q_y, Q_z, 1) \quad (7)$$

2.3 Milling surface topography simulation algorithm

After modelling the machining process, this section discretizes the cutting edge and machining time, meshes the workpiece, and solves the residual height of the workpiece surface by comparing the height values of the discretized points of the cutting edge with the mesh points of the workpiece, to realize the simulation of milling surface topography.

To ensure the simulation accuracy, the discretization accuracy of the cutting edge and machining time needs to be ensured, which is related to the accuracy of the workpiece meshing. As shown in Fig. 3, the workpiece's surface is discretized into a $m \times n$ rectangular grid, and to make the discrete points on the cutting edge traverse all the grid points, it is necessary to keep the length L smaller than the minimum distance between workpiece grids. At the same time, to make the simulation more accurate, it is necessary to ensure that the projection (arc length AC) of the trajectory travelled by each discrete point on the cutting edge in a single time step Δt on the mesh surface of the workpiece is less than $min\{dx, dy\}$. Therefore, the microelement length L of the cutting edge as well as the single time step Δt should satisfy the following formulation:

$$L \le min(dx, dy), dx = lx/m, dy = ly/n \quad (8)$$

$$\Delta t \le \frac{min\{dx, dy\}}{v}, v = 2\pi\cdot r\cdot n/60 \quad (9)$$

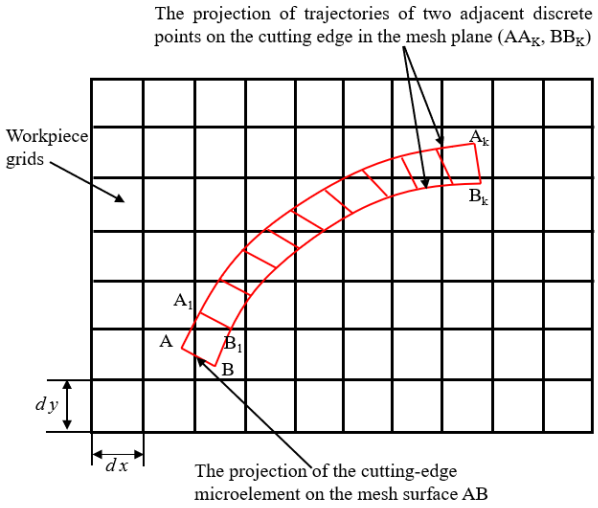

Fig. 3. Grid diagram of the milled workpiece.

In Eq. (8), L is the length of a single cutting-edge microelement, dx and dy are the length and width of the discretized mesh, lx and ly are the length and width of the workpiece respectively; In Eq. (9), Δt is a single time step, v is the linear velocity of a discrete point on the cutting-edge, and n is the rotational speed.

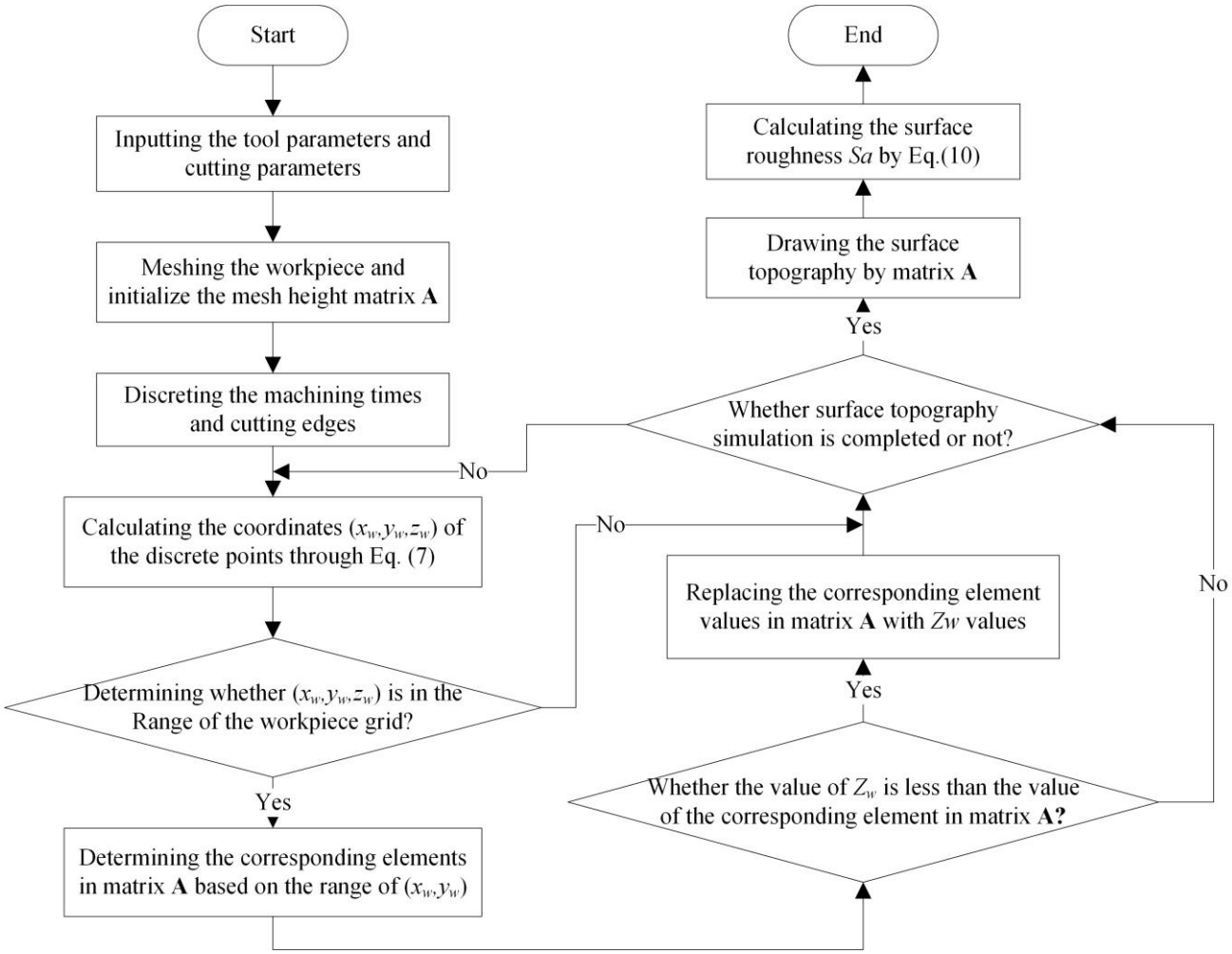

Fig. 4. the flow chart of the algorithm for milling surface topography.

After the machining time and the cutting edge are discretized according to the corresponding accuracy, the position of the discrete point on the cutting edge at any moment in the coordinate system of the workpiece can be calculated by Eq. (7). Compared with the height value of the workpiece, if the height of the discrete point is smaller than the height value on the workpiece's surface, it indicates that the workpiece is machined, and the height of the point on the workpiece surface needs to be updated. On the contrary, if the height value of the discrete points is larger than the height value of the workpiece surface, it indicates that the workpiece is not milled and the height of the workpiece surface does not need to be changed. The specific simulation steps are as follows:

(1) Initialize milling data. Setting the geometric and milling parameters of the tool (including the radius of the tool, the number of teeth of the tool, the row spacing, the feed per tooth, the spindle speed, etc.).

(2) Establish the workpiece mesh model. According to the size of the workpiece, the workpiece is meshed and the matrix $A[i,j](i = 1,2,\cdots,m; j = 1,2,\cdots,n)$ is used to denote the height corresponding to each mesh point on the surface of the part.

(3) Discrete process. The machining time of the workpiece and the milling edge of the tool are discretized according to the corresponding accuracy.

(4) Machining area judgment. Calculate the coordinate value (x_w, y_w, z_w) of the discrete point on the cutting edge in the workpiece coordinate system at the current moment, and judge whether the discrete point on the tooth enters the cutting area of the workpiece by the coordinate value: if $0 \le x_w \le lx$ and $0 \le y_w \le ly$ are satisfied at the same time, the point has entered the cutting area of the workpiece; otherwise, the calculation of the next discrete point is carried out.

(5) Correspondence between discrete and grid points. The corresponding relationship between the discrete points of the cutting edge and the grid points of the workpiece is determined

by the correspondence between the coordinate value (x_w, y_w) and the subscripts (i, j) of the height matrix $\boldsymbol{A}$. When the coordinate value (x_w, y_w) of the discrete point falls on the grid point, it is indicated that the point exactly corresponds to an element of the matrix $A[i, j]$;when the coordinate value (x_w, y_w) of discrete point is not on the grid point, it is sufficient to find its nearest workpiece grid point.

(6) Cutting judgment. Compare the value z_w with the element $A[i, j]$ of the corresponding height matrix $\boldsymbol{A}$. If z_w is small, the workpiece is cut, and replace $A[i, j]$ with z_w and store the value in matrix $\boldsymbol{A}$; Otherwise, it will not be processed.

(7) Topography generation. According to the final data stored in the matrix $\boldsymbol{A}$, the surface topography is gained by using simulation software.

(8) Calculation of surface roughness. After the surface topography simulation is completed, according to the definition of three-dimensional (3D) arithmetic mean deviation [32], the surface roughness (*Sa*) can be represented as:

$$Sa = \frac{1}{mn}\sum_{u=1}^{m}\sum_{v=1}^{n}|z(u,v) - h| \tag{10}$$

where m and n are the number of discrete points in X and Y directions respectively, $z(u, v)$ is the height of the discrete point, and h is the reference plane equation. The reference plane is the three-dimensional arithmetic mean plane, and the equation $h = \frac{1}{mn}\sum_{u=1}^{m}\sum_{v=1}^{n} z(u, v)$.

3. Surface roughness prediction model based on sparrow search algorithm optimized least support square vector machine method

As an important index to measure the quality of machined parts, surface roughness prediction is particularly important in practical machining. This part acquires a massive amount of data from the simulation and establishes a prediction model about *Sa* in combination with the Least Support Squares Vector Machine (LSSVM) for predicting 3D surface roughness. The accuracy of the prediction model based on LSSVM depends largely on the parameters σ and γ in the LSSVM model. However, the SSA algorithm has the characteristics of strong search ability and fast speed, which is beneficial for the optimization of parameters in LSSVM. Therefore, SSA-LSSVM is used to establish the prediction model of surface roughness in this section, which makes the prediction of surface roughness intelligent and precise.

3.1. Least-squares support vector machine (LSSVM)

Support Vector Machine (SVM) is a machine learning algorithm proposed by Vapanik et al [33], which has good predictive ability in dealing with nonlinear complex and finite sample information, but with high computational complexity, long learning time, and low efficiency. The Least Squares Support Vector Machine (LSSVM) is an improvement of SVM by adding the sum of error squares to the objective function [34]. Compared with SVM, LSSVM applies a new function, which can accurately find the analytical solutions of the model parameters, improve the computational efficiency, and has strong nonlinear fitting ability and. Therefore, this study proposes to use LSSVM to establish the prediction model of surface roughness.

Assume that the sample data is (x_i, y_i), $x_i \in R^n$ is the input variable, which is the parameter affecting the surface roughness, and $y_i \in R$ is the corresponding output value, which is the 3D surface roughness, where R^n and R are the n-dimensional vector and the one-dimensional vector respectively. The expression for the regression prediction of the LSSVM is given by:

$$y = f(x) = \omega^T \cdot \phi(x) + b \tag{11}$$

where ω^T is a multidimensional feature space weight vector, b is a constant, and $\phi(x)$ is a nonlinear mapping function. By the SVM theory, Eq (12) can be given to solve Eq. (11):

$$min\, J(\omega, e) = \frac{1}{2}||\omega||^2 + \frac{1}{2}\gamma\sum_{i=1}^{n} e_i^2 \,, st. \omega^T\phi(x_i) + b + e_i = y_i, i = 1,2\cdots n \tag{12}$$

where e_i is the deviation between the output and the result of the regression function, γ is the regularization parameter.

To solve the above optimization problem, the corresponding Lagrangian function is constructed and transformed as:

$$L(\omega, b, e, \alpha) = \frac{1}{2}||\omega||^2 + \frac{1}{2}\gamma\sum_{i=1}^{n} e_i^2 - \sum_{i=1}^{n}\alpha_i(\omega^T\phi(x_i) + b + e_i - y_i) \tag{13}$$

where $\alpha = [\alpha_1, \alpha_2, \cdots, \alpha_n]$ is the Lagrangian vector, α_i is the Lagrangian multiplier.

According to the Karush-Kuhn-Tucker condition, the partial derivatives of $L(\omega, b, e, \alpha)$ in Eq. (13) can be obtained and make its value zero, as shown in Eq. (14):

$$\frac{\delta L}{\delta \omega} = 0 \rightarrow \omega = \sum_{i=1}^{n} \phi(x_i), \frac{\delta L}{\delta b} = 0 \rightarrow \sum_{i=1}^{n} \alpha_i, \frac{\delta L}{\delta e_i} = 0 \rightarrow$$

$$e_i = \frac{\alpha_i}{r}, \frac{\delta L}{\delta \alpha_i} = 0 \rightarrow \omega^T \phi(x_i) + b + e_i - y_i = 0 \quad (14)$$

Eliminating ω and e_i, the solution to Eq. (14) is expressed as:

$$\begin{bmatrix} 0 \\ y \end{bmatrix} = \begin{bmatrix} 0 & V^T \\ V & K + \gamma^{-1} I \end{bmatrix} \begin{bmatrix} b \\ \alpha \end{bmatrix} \quad (15)$$

where $\alpha = [\alpha_1, \alpha_2, \cdots, \alpha_n]$, $y = [y_1, y_2, \cdots y_n]^T$, $Q = [1,1, \cdots 1]^T$, I is the unit matrix, and $K(x_i, y_i)$ is the kernel function, which is calculated as:

$$K(x_i, x_j) = exp(\frac{||x_i - x_j||}{2\sigma^2}) \quad (16)$$

In conclusion, the final LSSVM model is presented as:

$$y = \sum_{i=1}^{n} \alpha_i K(x_i, x_j) + b \quad (17)$$

3.2. Sparrow Search Algorithm (SSA)

The sparrow search algorithm, an intelligent optimization algorithm inspired by the sparrow's foraging behaviour and predator avoidance behaviour [35], was proposed in 2020. It is a new model and provides the advantages of high optimization ability and speed [36]. The sparrow search algorithm mainly simulates the process of sparrow feeding, and each sparrow represents a location attribute.

In D-dimensional space, the position of each sparrow $X_{site} = [X_1, X_2, \cdots, X_D]$, the fitness value $f = [f_1, f_2, \cdots, f_d]$, and the fitness function is selected to be the mean-square error as shown in Eq. (18).

$$e_{mse} = \sqrt{\frac{1}{n} \sum_{k=1}^{n} (y - y')^2} \quad (18)$$

Where y is the expected value and y' is the predicted value.

The sparrow algorithm operation process consists of three parts: discoverer, follower and pre-warner, in which the total number and proportion of discoverers and followers are unchanged, and the two can be transformed into each other according to the change of the fitness value. The optimal positions of the population members are constantly updated by foraging and anti-predation behaviors.

Set the number of sparrow populations to N. In the K-th iteration, the position of the discoverer is updated in the manner as:11

$$x_{i,p}^{k+1} = \begin{cases} x_{i,p}^{k} \cdot exp(\frac{-i}{\alpha \cdot G}), R < S \\ x_{i,p}^{k} + Q \cdot M, R > S \end{cases} \quad (19)$$

Where $x_{i,p}^{k+1}$ denotes the information of the i-th sparrow in the j-th dimension in the p-th iteration. G is the maximum number of iterations, Q is a random number obeying the standard normal distribution, M is a unit vector, and R and S stand for the warning value and the safety value, respectively. When $R < S$, it means that there is no danger near the search range and the search range continues to expand. On the contrary, danger is found near the search range and the position needs to be moved.

The follower's position is updated in the following way:

$$x_{i,p}^{k+1} = \begin{cases} Q \cdot exp(\, xw_p^k - x_{i,p}^k), i > \frac{n}{2} \\ xb_p^{k+1} + |x_{i,p}^k - xb_p^{k+1}| \cdot A \cdot M, i < \frac{n}{2} \end{cases} \quad (20)$$

Where xw_p^k is the global worst value for that iteration, xb_p^{k+1} denotes the optimal position of the current finder.

The proportion of pre-warners in the population is between 10% and 20%, and the location is updated as below:

$$x_{i,p}^{k+1} = \begin{cases} x_{best}^k + \beta \cdot (x_{i,p}^k - x_{best}^k), f_i > f_g \\ x_{i,p}^k + \lambda \cdot (\frac{|x_{i,p}^k - xw_p^k|}{(f_i - f_w) + \varepsilon}), f_i = f_g \end{cases} \quad (21)$$

Where x_{best}^k is currently the best place for sparrows, β is a parameter about the step, $\lambda \in [-1,1]$, f_i is the current individual fitness value, f_g and f_w are the current population optimal fitness and worst fitness respectively.

3.3. Surface roughness prediction model by the SSA-LSSVM

When using the LSSVM method to build the model of roughness prediction, it is necessary to choose the appropriate kernel width coefficient σ and regularization parameter γ , which is the key to accurate prediction. Hence, in this section, the sparrow search algorithm is applied to find the optimal values of parameters σ and γ to improve the prediction accuracy. The steps of the algorithm are displayed below:

1 Acquire the data, divide the training and test samples, and normalize the data by Eq. (22).

$$u_i' = \frac{u_i - u_{min}}{u_{max} - u_{min}} \quad (22)$$

where u_i' denotes the normalized data; u_i is the original data; u_{max} and u_{min} are the maximum and minimum values in the original data, respectively.

2 Initialize the parameters of the SSA-LSSVM model, including the population size, the iteration number, the proportion of discoveries and followers, and the ranges for

(σ, γ).

3 The initial fitness value f of each sparrow is calculated according to Eq. (18) and ranked according to the fitness size.

4 Based on Eq. (19) to (21), the positions of the discoverer, follower, and pre-warner are updated, the fitness value of the sparrow's new position is calculated, and fg as well as fw are updated.

5 Determine whether the maximum iteration number is reached or not. If reached then output the global optimal parameters, otherwise go to step 4.

6 The best value (σ, γ) searched by SSA is assigned to LSSVM and the LSSVM model is trained to obtain an optimized prediction model about Sa.

The flow chart for Sa prediction model is shown in Fig. 5.

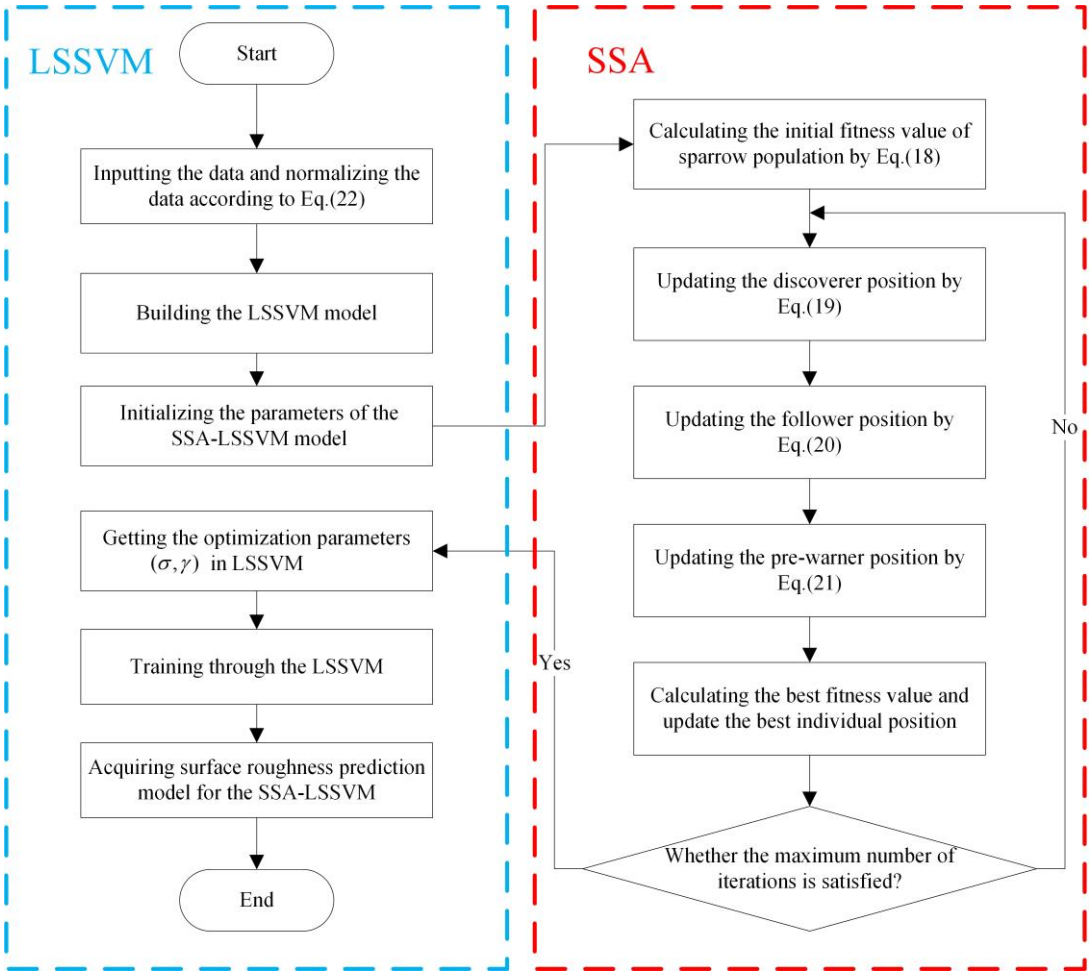

Fig. 5. The flowchart to predict the surface roughness by SSA-LSSVM.

The surface topography modelling and the surface forming mechanism in the second part of this paper showed that feed per tooth, row spacing, tool radius, and rake angle are the key contributors affecting surface roughness.

In this section, feed per tooth, row spacing, tool radius, and forward tilt angle are used as inputs, and surface roughness is the output value. To improve the accuracy of the prediction model, the training samples should be as large as possible and four values are selected for each of the above parameters as shown in Table 2. Considering the coupling effect of various factors, a total of $4^4 = 256$ sets of results are obtained through simulation experiments, as shown in Table 3. Therefore, 256 groups of data were obtained, in which 226 groups were randomly selected to train the model, and the remaining 30 groups were used to evaluate the effect of the SSA-LSSVM model.

Table 2. Values of input parameters.

No.	Input parameter	Input value
1	Feed per tooth (mm/z)	0.2，0.3，0.4，0.5
2	Row spacing (mm)	0.2，0.3，0.4，0.5
3	Tool radius (mm)	3，4，5，6
4	Forward tilt angle (°)	0，5，10，15

Table 3. Simulation results.

Feed per tooth(mm/z)	Row spacing(mm)	Tool radius(mm)	Forward tilt angle (°)	surface roughness (um)
0.2	0.2	3	0	1.0003
0.2	0.3	3	0	1.4185
0.2	0.4	3	0	1.9329
0.2	0.5	3	0	2.6059
0.3	0.2	3	0	1.2263
0.3	0.3	3	0	2.341
0.3	0.4	3	0	3.0329
0.3	0.5	3	0	3.4444
⋮	⋮	⋮	⋮	⋮
0.4	0.2	6	15	0.9253
0.4	0.3	6	15	0.9914
0.4	0.4	6	15	1.1855
0.4	0.5	6	15	1.4963
0.5	0.2	6	15	1.502
0.5	0.3	6	15	1.5461
0.5	0.4	6	15	1.6507
0.5	0.5	6	15	1.8702

3.4. Predictive results and analysis of the model

The above 256 sets of simulation experimental data are numbered, and 226 sets of them are chosen for training. The parameters of SSA-LSSVM are set as shown in Table 4, and the iterative process of seeking the optimal parameters in the LSSVM by SSA is presented in Fig. 6

Table 4 The parameters of SSA-LSSVM

parameters	value
sparrow populations	30
the maximum number of iterations	40
σ	[0.01, 100]
γ	[0.1, 2000]
safety value	0.6
Proportion of discoverers in the population	0.7
Proportion of followers in the population	0.1
Proportion of pre-warner s in the population	0.2

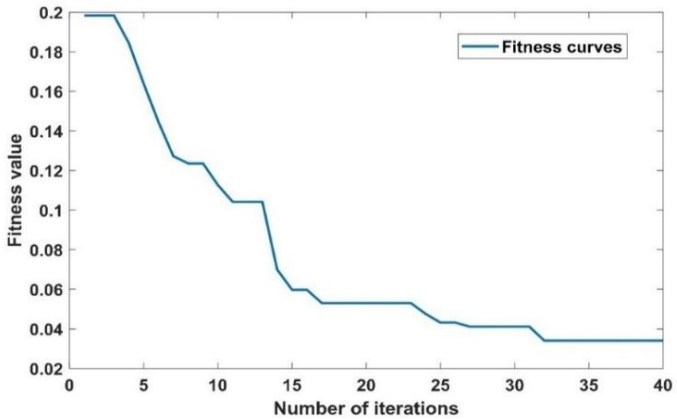

Fig. 6. Fitness curve by the SSA-LSSVM.

To effectively analyze and evaluate the of the effectiveness of the proposed model, the paper uses five performance indexes by comparing real and predicted data, and they are calculated as in Eqs. (23-27).

$$REA(Absolute\ value\ of\ relative\ error) = \frac{|R_i - P_i|}{R_i} \quad (23)$$

$$REA(Nash\ effciency) = 1 - \frac{\sum_{i=1}^{N}(R_i - P_i)^2}{\sum_{i=1}^{N}(R_i - \bar{R})^2} \quad (24)$$

$$RMSE(Root\ mean\ square\ error) = \sqrt{\frac{\sum_{i=1}^{N}(R_i - P_i)^2}{N}} \quad (25)$$

$$MAE(Mean\ absolute\ error) = \frac{1}{N}\sum_{i=1}^{N}|R_i - P_i| \quad (26)$$

$$WI(Willmott\ index) = 1 - \frac{\sum_{i=1}^{N}(R_i - P_i)^2}{\sum_{i=1}^{N}(|R_i - \bar{R}| + |P_i - \bar{R}|)^2} \quad (27)$$

where R_i is the actual surface roughness value and P_i is the predicted surface roughness value; $\overline{R}$is the mean value of the predicted surface roughness in the data, N is the total number of test samples. The REA, RMSE and MAE are closer to 0, and the NSE and WI are closer to 1, indicating the effect of the model is better.

Fig. 7 (a) compares the predicted and actual results of SSA-LSSVM. The blue points show the relationship between the predicted and actual values in the test samples. The red line indicates “Predicted value of surface roughness = Actual value of surface roughness”, and the closer the blue points are to the red line, the smaller the error from the prediction model. As shown in Fig. 7 (a), most of the blue dots are very close to the red line, demonstrating the correctness of the roughness prediction model developed in the paper.

To further illustrate the superiority of the model in the paper, the paper applys the LSSVM, the PSO-LSSVM and the WOA-LSSVM to compare with the SSA-LSSVM. The sample data, inputs, and outputs of each prediction model are the same as those of the SSA-LSSVM model. The prediction results of each model for the test samples are shown in Figs.7 (b-d), and the performance indexes of each model are presented in Table 5.

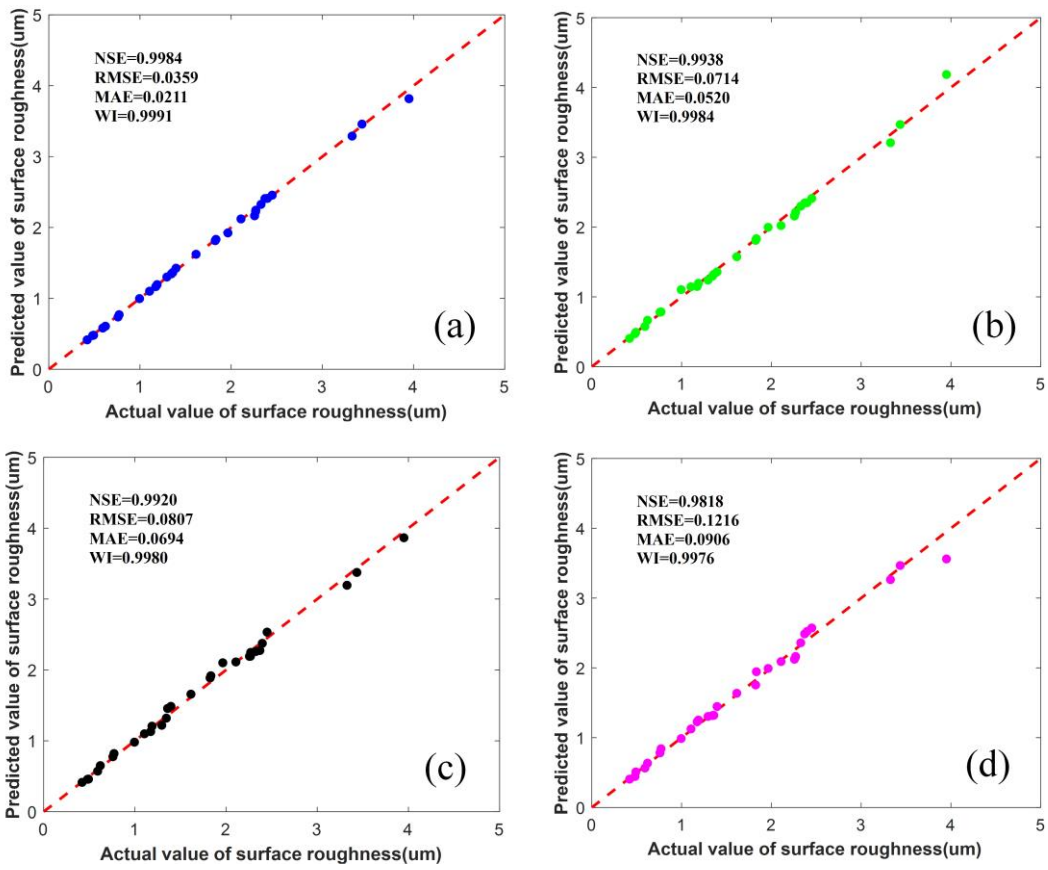

Fig. 7. Scatter plot of predicted and actual values by different prediction model: (a) SSA-LSSVM (b) PSO-LSSVM (c) WOA-LSSVM (d) LSSVM.

Table 5. Performance indexes of each model.

Indexes \ Method	SSA-LSSVM	PSO-LSSVM	WOA-LSSVM	LSSVM
NSE	0.9984	0.9938	0.9920	0.9818
RMSE	0.0359	0.0714	0.0807	0.1216
MAE	0.0211	0.0520	0.0694	0.0906
WI	0.9991	0.9984	0.9980	0.9976

As shown in Fig. 7, the SSA-LSSVM prediction model developed in the paper is closer to the actual results than the other models, which indicates its better prediction performance. As shown in Table 5, the performance indexes RMSE and MAE in the SSA-LSSVM are 0.0359 and 0.0211, which are smaller than those of other models, and the NSE and WI are 0.9984 and 0.9991, respectively, which are closer to 1 than those of other models. This further proves that the prediction results of the SSA-LSSVM model have a higher precision accuracy.

In addition, Figs 8 and 9 show the Violin and Taylor diagrams for the different models. The Taylor diagram shows that the predicted values obtained by SSA-LSSVM have a closer standard deviation and higher correlation with the actual values. The violin diagram shows the method proposed in the paper seems to be more similar to the distribution of actual values compared to the other methods. Fig 10 compares the absolute value of the relative error (REA) of each model. It can be seen that the REA of the SSA-LSSVM model is overall lower than the REA of the other models, and the REA curve fluctuates around 0, further showing the superiority of the SSA-LSSVM model. Therefore, the SSA-LSSVM method proposed in the paper has a greater advantage in surface roughness prediction.

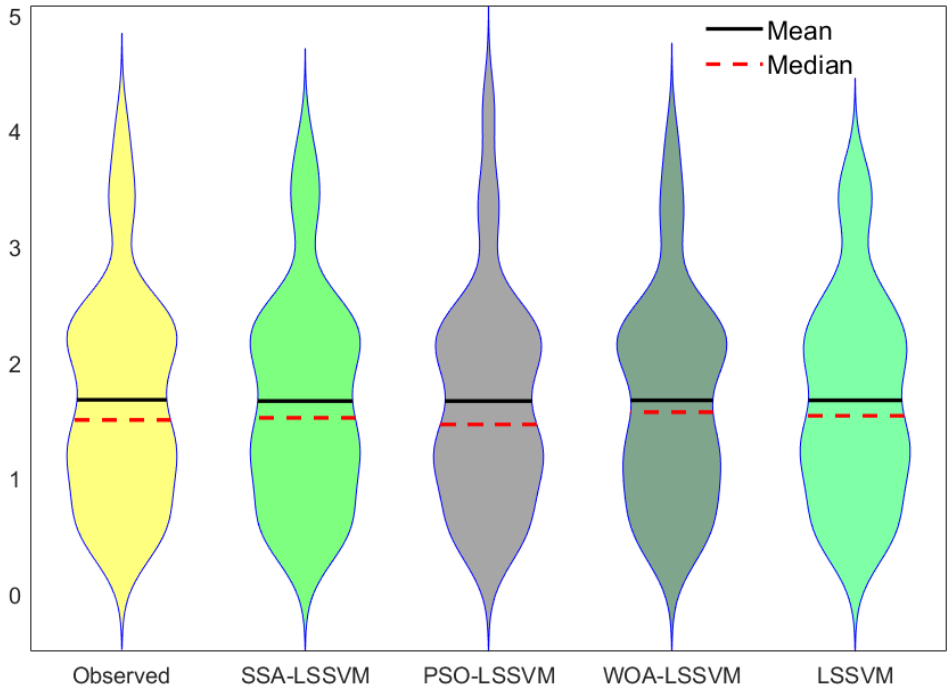

Fig. 8. Violin diagram of different models.

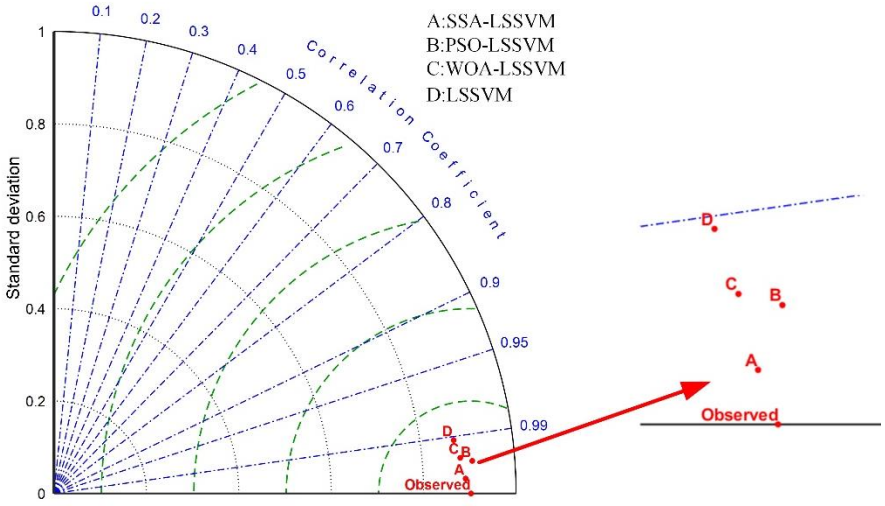

Fig. 9. Taylor diagram of different models.

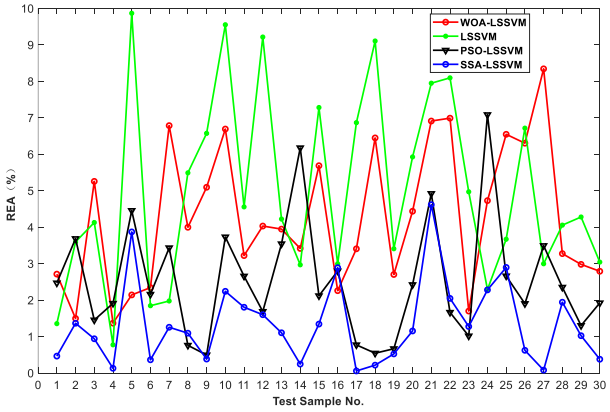

Fig. 10. The absolute value of relative error between predicted and actual values.

4. Reliability model of surface roughness based on response surface method

From the modelling of the surface topography above, it is clear that the surface topography is affected by the feed per tooth, the row spacing, the tool radius, and the tool rake angle, which also affects the surface roughness. In practical machining, the small fluctuations in the milling process are not considered, which inevitably results in small variations in cutting parameters. These variations can further lead to uncertainty in surface roughness, which may result in surface quality failure due to substandard surface roughness. Hence, it is essential to develop

the research on surface roughness reliability.

Most of the existing reliability calculation methods are based on the known functional expressions, and the reliability is obtained by the primary second-order moments, JC method, Monte Carlo method and other methods [37]. However, in some practical problems, such as for nonlinear systems like the one in this paper, the relationship between the fundamental random variables and *Sa* may be highly nonlinear, and there is no clear analytical expression [38]. When calculating the reliability of such systems, the above method may not be possible to calculate the reliability. The surface roughness in this paper has a nonlinear relationship with feed per tooth, row spacing, tool radius, and tool rake angle, no explicit expression exists. Therefore, this section analyzes surface roughness reliability through the response surface methodology, which provides a solution to the problem of reliability analysis of such complex systems.

The response surface methodology uses the experimental design method to generate sample points by inputting a certain range of parameter values, fitting a response surface function using regression analysis, and replacing the real function or limit state surface with an easy function (response surface function) or surface (response surface) to complete the reliability calculation [39,40].

Response surface functions are usually often in polynomial form for the basic random variable and are generally expressed as a noncomplete quadratic polynomial that ignores the cross-product term. The response surface function for n random variables is usually expressed as:

$$g = Z(x) = a_0 + \sum_{i=1}^{n} b_i x_i + \sum_{i=1}^{n} c_i x_i^2 \tag{28}$$

where x is the underlying random variable; $Z(x)$ is the response surface function; a_0, b_i and c_i are $2n$+1 coefficients to be determined.

The design variables in this section are feed per tooth, row spacing, tool radius, and tool rake angle, respectively, which are expressed in the form of a random vector $x = [x_1, x_2, \cdots, x_n]$. The steps to obtain reliability based on the response surface methodology are given as follows:

(1) The number of variables n is determined and the response surface function form as shown in Eq. (28) is chosen.

(2) According to the center point of this iteration, the sample points are selected by following the central composite design method. Assuming that in the k-th iteration, with $X^{(k)} = (x_1^{(k)}, \cdots, x_i^{(k)}, \cdots x_n^{(k)})$ as the center point, $2n$ sample points are selected according to Eq. (29), and a total of $2n$+1 sample points are obtained by combining the center points $X^{(k)}$. where the center point of the first iteration $X^{(1)} = \mu_x = (\mu_1, \cdots, \mu_i, \cdots \mu_n)$, $\mu_x$is the mean point of the fundamental random variable.

$$X_{i\pm}^{(k)} = X^{(k)} \pm f\delta_i e_i \tag{29}$$

where δ_i is the standard deviation of the underlying random variable, f is the coefficient, which takes the values 1, 2, or 3, and $e_i = [0, \cdots 0,1,0 \cdots 0]$, where the i-th element is 1.

(3) According to the $2n$+1 sets of sample points, calculate the function function values for these points: $g = [g_1, g_2, \cdots, g_{2n+1}]$

(4) Since Eq. (28) has only 2n+1 coefficients to be determined, by bringing the data from steps (2) and (3) into the Eq. (28), the system of equations can be derived:

$$X\lambda^T = Y \tag{30}$$

where $\lambda = (a_0, b_1, \cdots, b_n, c_1, \cdots, c_n)$, $Y = (g_1, g_2, \cdots, g_{2n+1})^T$.

(5) The JC method or the improved first second order moment is utilized to solve the check-point $X^{\Theta(K)} = (x_1^{\Theta(K)}, x_2^{\Theta(K)}, \cdots, x_n^{\Theta(K)})$ of $z(x)$ and the reliability index $\beta^{(K)}$, where the superscript K denotes the K-th iteration step.

(6) The center point $X^{(K+1)}$ of the next iteration is calculated by linear interpolation of the sample point $(X^{(K)}, z(X^{(K)}))$ and the check-point $(X^{\Theta(K)}, z(X^{\Theta(K)}))$, $X^{(K+1)}$ is calculated by Eq. (31):

$$X^{(K+1)} = X^{(K)} + (X^{\Theta(K)} - X^{(K)}) \cdot \frac{z(X^{(K)})}{z(X^{(K)}) - z(X^{\Theta(K)})} \tag{31}$$

(7) With the new $X^{(K+1)}$ as the center point, continue with steps (2) to (5) to find the reliability indicators $\beta^{(K+1)}$ for the $(k+1)$-th time.

(8) Taking $| \beta^{(K)} - \beta^{(K+1)} | < \varepsilon$ as the condition to judge whether conversion or not, when the condition is satisfied, $\beta^{(K+1)}$ is the index of roughness reliability, and the calculation is finished; when the condition is not satisfied, continue the cycle of calculation until $| \beta^{(K)} - \beta^{(K+1)} | < \varepsilon$ is satisfied. The flow chart for solving roughness reliability based on the response surface method is shown in Fig. 11.

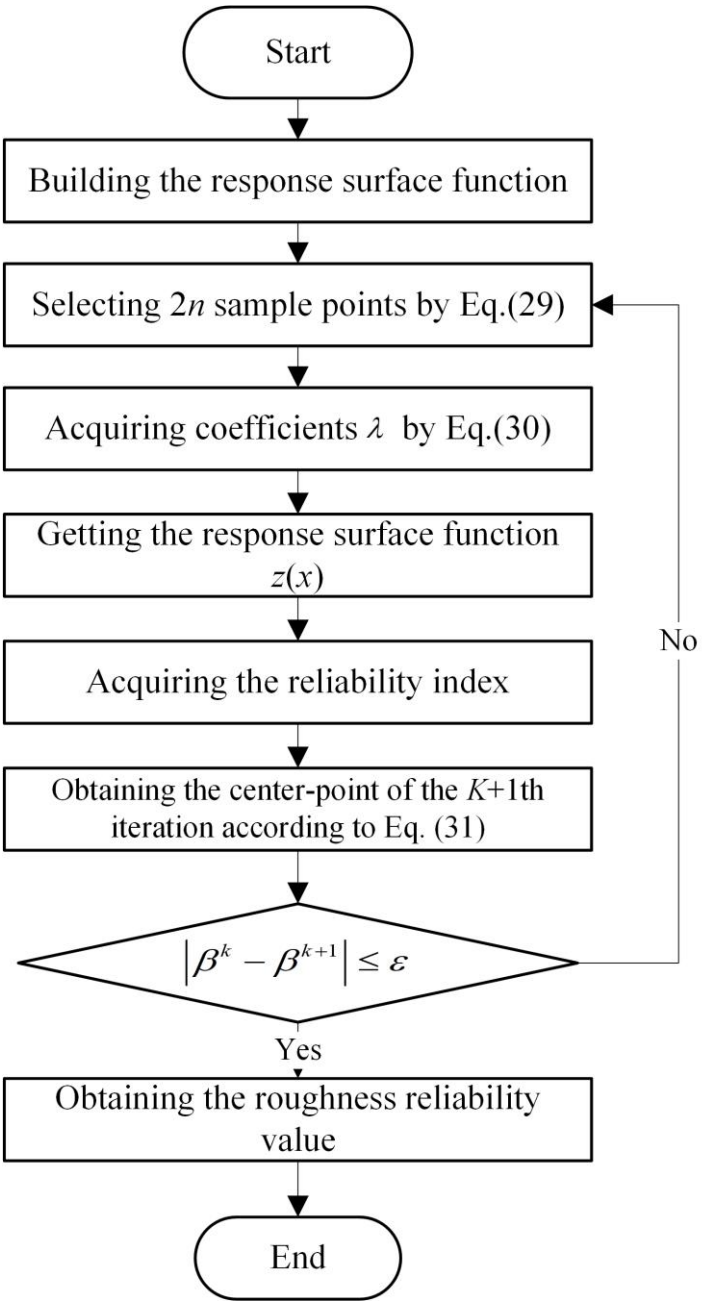

Fig. 11. The flow chart for calculating reliability by response surface methodology.

5. Experiment case

5.1. Experimental verification of surface topography and roughness

To verify the accuracy of the surface topography and surface roughness model, the paper adopts the orthogonal experimental program shown in Table 6, and conducts 16 sets of milling machining experiments on a four-axis machine tool. The material of the workpiece is aluminium alloy 7050, and the tool parameters appear in Table 7.

Table 6. Orthogonal experimental program.

NO.	Radius of the milling cutter(mm)	Row space(mm)	Feed per tooth(mm/r)	Tool front tilt angle(°)
1#	3	0.2	0.2	0
2#	3	0.3	0.3	5
3#	3	0.4	0.4	10
4#	3	0.5	0.5	15
5#	4	0.2	0.3	10
6#	4	0.3	0.2	15
7#	4	0.4	0.5	0
8#	4	0.5	0.4	5
9#	5	0.2	0.4	15
10#	5	0.3	0.5	10
11#	5	0.4	0.2	5
12#	5	0.5	0.3	0
13#	6	0.2	0.5	5
14#	6	0.3	0.4	0
15#	6	0.4	0.3	15
16#	6	0.5	0.2	10

Table 7. Tool parameters.

Radius of the milling cutter(mm)	Helix angle of tool (°)	Number of tool teeth	Total length of the tool(mm)
3 4 5 6	30	2	50

Fig. 12 shows the milling experimental machining site and workpiece after milling. In Fig. 12(b), the number of the machined workpiece corresponds to the number of each group of machining parameters.

Fig. 12. Milling site and finished workpieces:(a) Milling processing; (b) Workpieces after machining.

As shown in Fig. 13, the measuring instrument used for the

experiment, roughness profiler, has a measuring range of 0.01-10um, and the maximum travel distances in the horizontal and vertical directions are 100 mm and 80 mm respectively. After the milling process is completed, the measuring area is selected for each workpiece, and the roughness profiler is used to measure the height coordinates of the area and calculate the surface roughness *Sa* by Eq. (10).

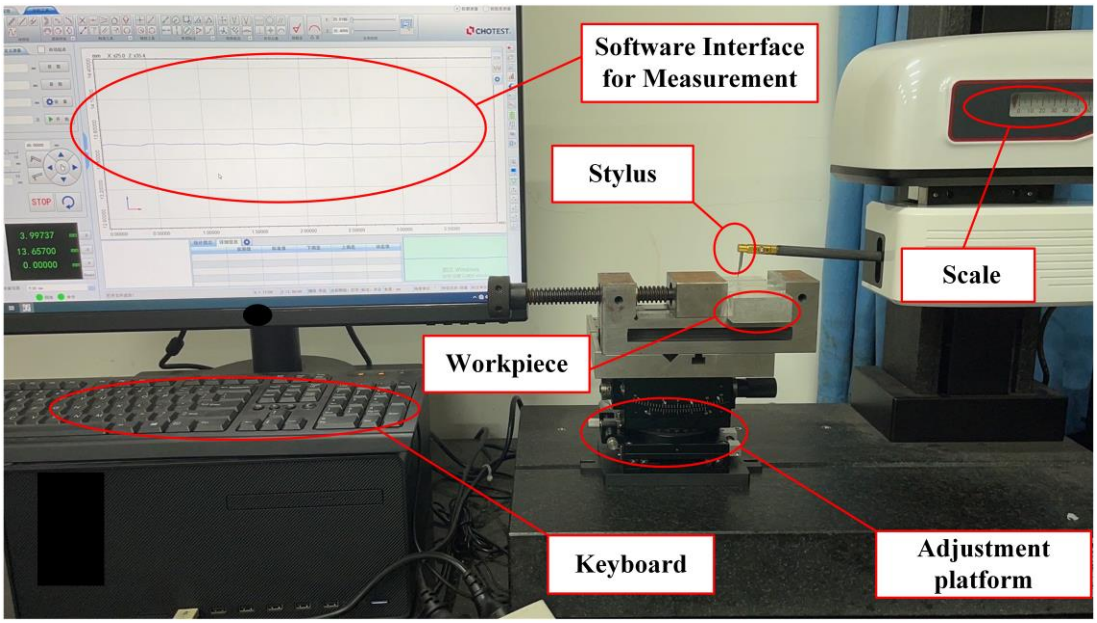

Fig. 13. Measuring process by roughness profiler.

Fig. 14 is a comparison of the experiment results with the measurement results, and it can be found that the *Sa* values obtained from the experiments under different milling conditions are the same as those obtained from the simulation. The maximum error value 9.84% occurs in group 4 and the error values of both experiment and simulation results are less than 10%. Therefore, the correctness of the method introduced in this paper are verified.

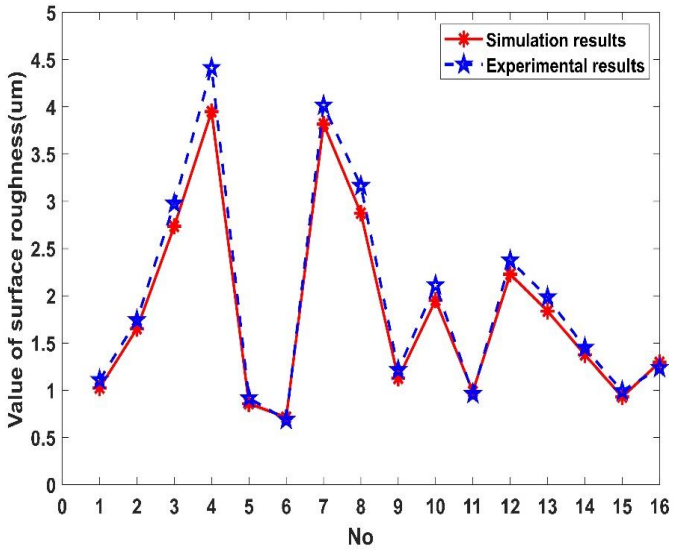

Fig. 14. Comparison of Experimental Results and Simulation Results.

To further illustrate the consistency between the simulation and the experiment, 2 groups were selected from the above experiments, and the corresponding two-dimensional(2D) contours in the row spacing direction and the feed direction were intercepted to compare. With the acquired profile data, the root-mean-square error (RSME) between the simulation results and the measurement results is introduced as an evaluation parameter to assess the correctness of the model, and smaller RMSE values indicate higher correctness. The RMSE is represented by:

$$RMSE = \sqrt{\frac{\sum_{i=1}^{n}(Z(x_i,y_i)-Z(X_i,Y_i))^2}{n}} \tag{32}$$

where $Z(x_i, y_i)$ is the corresponding height of the simulated 2D profile, $Z(X_i, Y_i)$ is the height of the measured 2D profile corresponding to the simulation, and n is the total number of measurement points.

As shown in Figs. 15(a)-(d), the 2D contour diagrams of simulation and experiment for the parameter cases of group 3 and group 12, respectively, it is observed that the 2D contour change trends of simulated and experimental results are generally the same. As can be seen from Figs. 15(b) and (d), the corresponding row spacings are 0.4 mm and 0.5 mm, respectively, which are consistent with the parameters of the

milling experimental row spacings, further demonstrating the consistency between simulation and experiment.

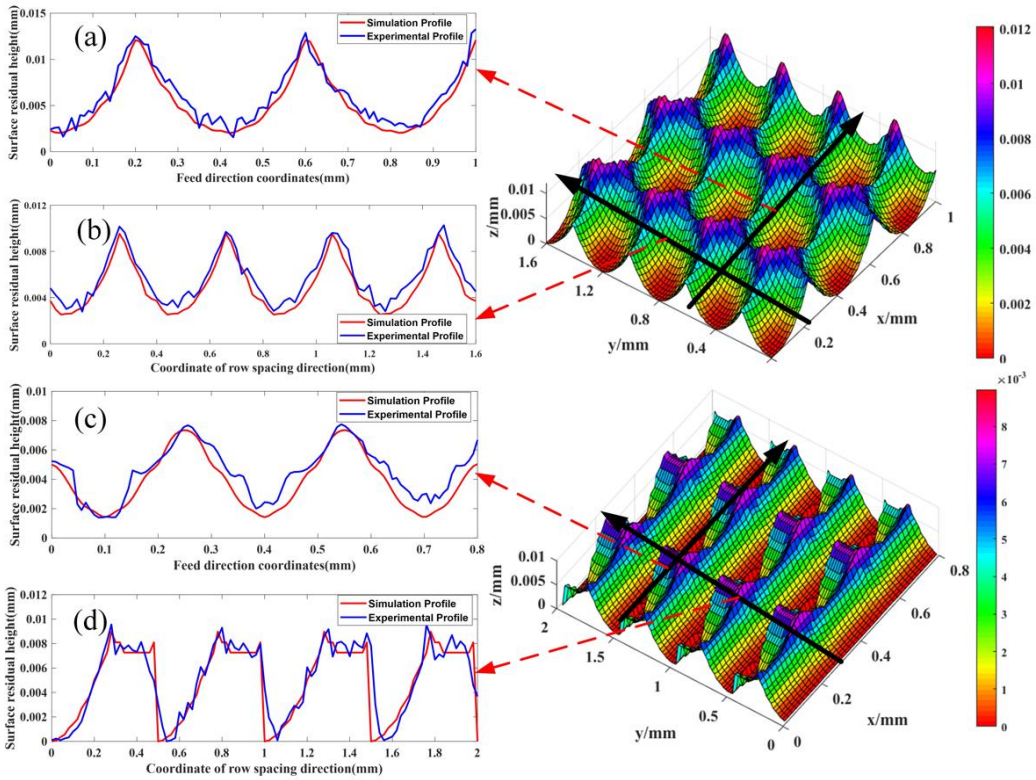

Fig. 15. Comparison of 2D contours of simulation results and experimental results (a) Feed direction contour under group 3 parameters; (b) Line spacing direction contour under group 3 parameters; (c) Feed direction contour under group 12 parameters; (d) Line spacing direction contour under group 12 parameters.

By Eq (30), the corresponding RMSE values of Figs. 15(a)-(d) can be obtained in Table 8, and it is evident that the RMSE values are all near 0, indicating that the deviation of the 2D profile between the simulation and the experiment is very minor, and the simulation and experiment are relatively consistent. Therefore, the surface topography simulation method and roughness prediction method proposed in this study have been experimentally verified, which can provide theoretical guidance for the prediction and improvement of the workpiece's surface quality.

Table 8. RMSE values corresponding to Figs. 15(a)-(d).

No.	RMSE
Figure a	0.000987
Figure b	0.000904
Figure c	0.000891
Figure d	0.0014

5.2 Experimental verification of roughness reliability

Surface roughness reliability can be used to evaluate whether the surface roughness or surface quality of several parts meets the actual production requirements. As shown in Fig. 16, the same roughness profiler above is used for the experimental verification of the roughness reliability.

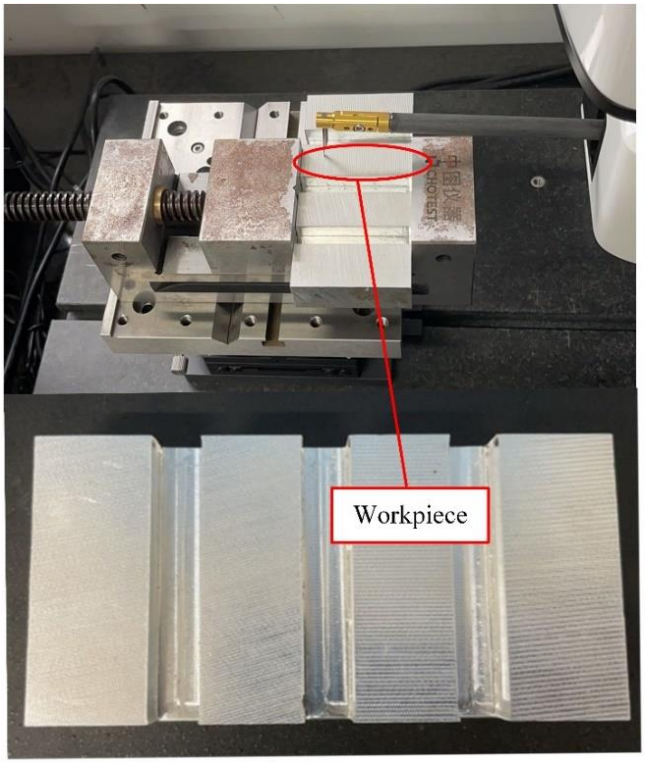

Fig. 16. Measurement of roughness reliability.

Before the measurement, the surface of the machined workpiece needs to be divided into 250 measurement areas of $2mm \times 2mm$. After the division of the area is completed, each area of the workpiece is measured with a roughness profiler to determine whether it is qualified or not according to whether the roughness of the area meets the permissible value, and then the roughness reliability in the actual situation is calculated by Eq. (33). By comparing the actual and simulated values of roughness reliability, it can demonstrate whether the surface roughness reliability model based on the response surface method is correct.

$$M_R = \frac{N_m}{N_n} \tag{33}$$

Where M_R is actual roughness reliability, N_m is measured area qualified quantity, N_n is total quantity of measurement area.

Table 9 shows that the roughness reliability model obtained by the method proposed in the paper is verified since the calculated values of reliability are particularly similar to the experimental results. By comparing with the Monte Carlo method, it is found that surface roughness reliability values acquired by this method are closer to the experimental values, demonstrating that the response surface method has a higher prediction precision than the Monte Carlo method. Therefore, the approach proposed in this study for obtaining roughness reliability by the response surface method was experimentally validated, and it can be used for roughness reliability prediction.

Table 9 Roughness reliability by various methods

No.	Methods for calculating reliability		Experimental methods for obtaining reliability		Reliability of the experiment
	response surface methodology	Monte Carlo method	Number of eligible areas	Total number of areas measured	
1	96.76%	95.85%	243	250	97.2%
2	95.63%	97.68%	238	250	95.2%
3	98.21%	96.73%	246	250	98.4%
4	97.09%	97.62%	241	250	96.4%
5	98.24%	96.51%	247	250	98.8%
6	97.56%	96.49%	243	250	97.2%
7	96.69%	98.19%	240	250	96.0%
8	98.06%	98.42%	244	250	97.6%
9	96.65%	95.61%	242	250	96.8%
10	96.93%	97.96%	243	250	97.2.%
11	96.88%	95.83%	244	250	97.6%
12	95.67%	96.37%	237	250	94.8%
13	95.29%	96.13%	239	250	95.6%
14	96.73%	97.54%	240	250	96%
15	94.58%	95.62%	233	250	93.2%
16	97.53%	96.84%	245	250	98.0%

6. Conclusion

The article develops a surface roughness prediction model, and applies the roughness reliability model established based on the response surface method to realize the surface quality assessment in actual milling machining. The specific conclusions are as follows:

(1) Based on milling kinematics theory, a milling surface topography model is established in this paper by discretizing the milling edge and machining time, which takes the influence of various parameters into account. The model can be used for milling surface topography simulation.

(2) Optimizing the key parameters of the LSSVM model by the SSA, the prediction accuracy of roughness model is more than 95% and the model performance indexes are all superior to other models, indicating that the SSA-LSSVM model proposed in this paper is more competitive in predicting surface roughness.

(3) For the uncertainty characteristic of various parameters in the machining process, the paper applies the response surface

method to establish a roughness reliability model. The experimental results show that the accuracy of the reliability model based on the response surface method is higher than that of the Monte Carlo method, which indicates that this method can be used to analyze the roughness reliability and provide a basis for the assessment of surface quality in the actual milling process.

(4) The paper focuses on the study of surface quality assessment in CNC milling, which is mainly limited to CNC milling machining processes. The next study is to develop a series of methods for the surface quality assessment of other various kinds of CNC machining, such as turning, grinding and boring.

Acknowledgments

The research was sponsored by the National Natural Science Foundation of China (grant no.51905334, grant no.52305261 and grant no.12002186), Shanghai Sailing Program (grant no.19YF1418600), Beijing Union University (No. ZK80202101), R&D Program of Beijing Municipal Education Commission (KM202211417012), and the Open Foundation of National Key Laboratory of Strength and Structural Integrity (ASSIKFJJ202305002).

Reference

1. Dong Y, Li S, Li Yan, et al. Research on Modeling and Simulation of Surface Topography Obtained by Trochoidal Milling Mode with Ball End Milling Cutter[J]. Journal of Mechanical Engineering, 2018, 54(19): 212-223. DOI:10.3901/JME.2018.19.212.
2. Wang B, Wang Z, Hou Y, et al. Surface texture prediction and analysis of ball end milling cutter machining[J]. Machine Tools and Hydraulics, 2016, 044(013):1-5. (In Chinese).
3. Yuan L, Zeng S, Chen Z. Simultaneous prediction of surface topography and surface location error in milling[J]. Proceedings of the Institution of Mechanical Engineers, Part C: Journal of Mechanical Engineering Science, 2015, 229(10): 1805-1829. DOI:10.1177/0954406214547401.
4. Peng Z, Jiao L, Yan P, et al. Simulation and experimental study on 3D surface topography in micro-ball-end milling[J]. The International Journal of Advanced Manufacturing Technology, 2018, 96: 1943-1958. https://doi.org/10.1007/s00170-018-1597-6.
5. Zhang W, Hua B, Zhang L, et al. Modeling and simulation of Surface Topography in secondary milling with ellipsoid end milling cutter[J]. International Journal on Interactive Designand Manufacturing (IJIDeM), 2023: 1-14. https://doi.org/10.1007/s12008-023-01475-6.
6. Zhang C, Zhang H, Li Y, et al. Modeling and on-line simulation of surface topography considering tool wear in multi-axis milling process[J]. The International Journal of Advanced Manufacturing Technology, 2015, 77: 735-749. https://doi.org/10.1007/s00170-014-6485-0.
7. Bo L, Yanlong C, Wenhua C, et al. Geometry simulation and evaluation of the surface topography in five-axis ball-end milling[J]. The International Journal of Advanced Manufacturing Technology, 2017, 93: 1651-1667. https://doi.org/10.1007/s00170-017-0505-9.
8. Hao Y, Liu Y. Analysis of milling surface roughness prediction for thin-walled parts with curved surface[J]. The International Journal of Advanced Manufacturing Technology, 2017, 93: 2289-2297. https://doi.org/10.1007/s00170-017-0615-4.
9. Shujuan L, Dong Y, Li Y, et al. Geometrical simulation and analysis of ball-end milling surface topography[J]. The International Journal of Advanced Manufacturing Technology, 2019, 102: 1885-1900. https://doi.org/10.1007/s00170-018-03217-5.
10. Żurawski K, Żurek P, Kawalec A, et al. Modeling of Surface Topography after Milling with a Lens-Shaped End-Mill, Considering Runout[J]. Materials, 2022, 15(3): 1188. https://doi.org/10.3390/ma15031188.
11. Chen W, Zheng L, Xie W, et al. Modelling and experimental investigation on textured surface generation in vibration-assisted micro-milling[J]. Journal of Materials Processing Technology, 2019, 266: 339-350. https://doi.org/10.1016/j.jmatprotec.2018.11.011.
12. Buj-Corral I, Vivancos-Calvet J, Dominguez-Fernandez A. Surface topography in ball-end milling processes as a function of feed per tooth and radial depth of cut[J]. International Journal of Machine Tools and Manufacture, 2012, 53(1): 151-159. https://doi.org/10.1016/j.ijmachtools.2011.10.006
13. Xu J, Xu L, Geng Z, et al. 3D surface topography simulation and experiments for ball-end NC milling considering dynamic feedrate[J]. CIRP Journal of Manufacturing Science and Technology, 2020, 31: 210-223. https://doi.org/10.1016/j.cirpj.2020.05.011.
14. Zheng M, Dong Y, et al. Effect of inclination-angle of ball-milling cutter on surface morphology of hard aluminium alloy workpiece. [J] Lanzhou Univ Technol 2016, 42(4):36–41. (In Chinese)

15. Agrawal A, Goel S, Rashid W B, et al. Prediction of surface roughness during hard turning of AISI 4340 steel (69 HRC) [J]. Applied Soft Computing, 2015, 30: 279-286. https://doi.org/10.1016/j.asoc.2015.01.059.
16. Kong D, Zhu J, Duan C, et al. Bayesian linear regression for surface roughness prediction [J]. Mechanical Systems and Signal Processing, 2020, 142: 106770. https://doi.org/10.1016/j.ymssp.2020.106770.
17. Shahrajabian H, Farahnakian M. Modeling and multi-constrained optimization in drilling process of carbon fiber reinforced epoxy composite[J]. International Journal of Precision Engineering and Manufacturing, 2013, 14: 1829-1837. https://doi.org/10.1007/s12541-013-0245-1.
18. Ouyang H B. Deformation prediction based on BP artificial neural network of milling thin-walled aluminum alloy parts[J]. Applied Mechanics and Materials, 2014, 687-691: 492-495 https://doi.org/10.4028/www.scientific.net/AMM.687-691.492
19. Han J, Zhu J, Zheng W, et al. Influence of metal forming parameters on surface roughness and establishment of surface roughness prediction model[J]. International Journal of Mechanical Sciences, 2019, 163: 105093. https://doi.org/10.1016/j.ijmecsci.2019.105093
20. Liu C, Huang Z, Huang S, et al. Surface roughness prediction in ball screw whirlwind milling considering elastic-plastic deformation caused by cutting force: Modelling and verification[J]. Measurement, 2023, 220: 113365. https://doi.org/10.1016/j.measurement.2023.113365.
21. Li B, Tian X. An effective PSO-LSSVM-based approach for surface roughness prediction in high-speed precision milling[J]. Ieee Access, 2021, 9: 80006-80014. https://doi.org/10.1109/ACCESS.2021.3084617
22. Hong S, Yue T, Liu H. Vehicle energy system active defense: a health assessment of lithium-ion batteries[J]. International Journal of Intelligent Systems, 2022, 37(12): 10081-10099. https://doi.org/10.1002/int.22309
23. Hong S, Zeng Y. A health assessment framework of lithium-ion batteries for cyber defense[J]. Applied Soft Computing, 2021, 101: 107067.
24. Yuan X, Chen C, Lei X, et al. Monthly runoff forecasting based on LSTM–ALO model[J]. Stochastic environmental research and risk assessment, 2018, 32: 2199-2212. https://doi.org/10.1007/s00477-018-1560-y
25. Adnan R M, Mostafa R R, Dai H L, et al. Pan evaporation estimation by relevance vector machine tuned with new metaheuristic algorithms using limited climatic data[J]. Engineering Applications of Computational Fluid Mechanics, 2023, 17(1): 2192258. https://doi.org/10.1080/19942060.2023.2192258.
26. Adnan R M, Mostafa R R, Islam A R M T, et al. Estimating reference evapotranspiration using hybrid adaptive fuzzy inferencing coupled with heuristic algorithms[J]. Computers and Electronics in Agriculture, 2021, 191: 106541. https://doi.org/10.1016/j.compag.2021.106541.
27. Adnan R M, Dai H L, Mostafa R R, et al. Modelling groundwater level fluctuations by ELM merged advanced metaheuristic algorithms using hydroclimatic data[J]. Geocarto International, 2023, 38(1): 2158951.https://doi.org/10.1080/10106049.2022.2158951.
28. Adnan R M, Dai H L, Mostafa R R, et al. Modeling multistep ahead dissolved oxygen concentration using improved support vector machines by a hybrid metaheuristic algorithm[J]. Sustainability, 2022, 14(6): 3470. https://doi.org/10.3390/su14063470.
29. Lu X, Hu X, Wang H, et al. Research on the prediction model of micro-milling surface roughness of Inconel718 based on SVM[J]. Industrial Lubrication and Tribology, 2016, 68(2): 206-211.https://doi.org/10.1016/j.neucom.2015.08.124
30. Misaka T, Herwan J, Ryabov O, et al. Prediction of surface roughness in CNC turning by model-assisted response surface method[J]. Precision Engineering, 2020, 62: 196-203. https://doi.org/10.1016/j.precisioneng.2019.12.004
31. Pimenov D Y, Bustillo A, Mikolajczyk T. Artificial intelligence for automatic prediction of required surface roughness by monitoring wear on face mill teeth[J]. Journal of Intelligent Manufacturing, 2018, 29(5): 1045-1061. https://doi.org/10.1007/s10845-017-1381-8
32. Li, W, Shuyi G E, Hao S I, et al. Elliptical model for surface topography prediction in five-axis flank milling[J]. Chinese Journal of Aeronautics, 2020, 33(4): 1361-1374. https://doi.org/10.1016/j.cja.2019.06.007.
33. Yuan X, Wang Y, Zhang Y. Support vector machine inverse model control based on fuzzy control compensation[J]. Electronic Measurement and Instrumentation. 2007, 21(01): 39-43. (In Chinese).
34. Wang H, Hu Z, Zhang Y et al. Short-term wind speed combination prediction based on clustered empirical mode decomposition and least squares support vector machine[J]. Journalof Electrotechnology, 2014, 29(04): 237-245. (In Chinese).
35. Song C, Yao L, Hua C, et al. A water quality prediction model based on variational mode decomposition and the least squares support vector machine optimized by the sparrow search algorithm (VMD-SSA-LSSVM) of the Yangtze River, China[J]. Environmental monitoring and assessment, 2021, 193(6): 363. https://doi.org/10.1007/s10661-021-09127-6.

36. Yue, Y., Cao, L., Lu, D. et al. Review and empirical analysis of sparrow search algorithm. Artif Intell Rev 56, 10867–10919 (2023). https://doi.org/10.1007/s10462-023-10435-1.
37. Changcong, Z.; Zhenzhou, L.; Feng, Z.; Zhufeng, Y. An Adaptive Reliability Method Combining Relevance Vector Machine and Importance Sampling. Struct. Multidiscp. Optim. 2015, 52, 945–957. https://doi.org/10.1007/s00158-015-1287-z.
38. Ou Y, Wu Y, Cheng J, et al. Response Surface Method for Reliability Analysis Based on Iteratively-Reweighted-Least-Square Extreme Learning Machines[J]. Electronics, 2023, 12(7): 1741. https://doi.org/10.3390/electronics12071741.
39. Zhang Z, Hu X, Qi Y, et al. Geometric error allocation method for CNC machine tools based on vector projection response surface[J]. Journal of Jilin University (Engineering Edition),2022,52(2): 384-391. Doi:10.13229/j.cnki.jdxbgxb20211089.
40. Niu P, Cheng Q, Zhang T, et al. Hyperstatic mechanics analysis of guideway assembly and motion errors prediction method under thread friction coefficient uncertainties[J]. Tribology International, 2023, 180: 108275. https://doi.org/10.1016/j.triboint.2023.108275.